Check for updates

Author Manuscript

Title: Elucidation of Design Criteria for V-based Redox Mediators: Structure-Function Relationships that Dictate Rates of Heterogeneous Electron Transfer

Authors: Mamta Dagar; William W. Brennessel; Ellen M. Matson

This is the author manuscript accepted for publication. It has not been through the copyediting, typesetting, pagination and proofreading process, which may lead to differences between this version and the Version of Record.

To be cited as: 10.1002/chem.202400764

Link to VoR: https://doi.org/10.1002/chem.202400764

WILEY VCH

RESEARCH ARTICLE

Elucidation of Design Criteria for V-based Redox Mediators: Structure-Function Relationships that Dictate Rates of Heterogeneous Electron Transfer

Mamta Dagar,[a] William W. Brennessel,[a] and Ellen M. Matson*[a]

[a] M. Dagar, W.W. Brennessel, E.M. Matson
University of Rochester
Department of Chemistry, Rochester NY 14627, USA
E-mail: matson@chem.rochester.edu

Supporting information for this article is given via a link at the end of the document

Abstract: Redox mediators are attractive solutions for addressing the stringent kinetic stipulations required for efficient energy conversion processes. In this work, we compare the electrochemical properties of four vanadium complexes, namely $[V(acac)_3]$, $[V_6O_7(OMe)_{12}]$, $[^nBu_4N]_3[V_6O_{13}(TRIS^{NO2})_2]$, and $[^nBu_4N]_5[V_{18}O_{46}(NO_3)]$ in non-aqueous solutions on glassy carbon electrodes. The goal of this study is to investigate the electron transfer kinetics and diffusivity of these compounds under identical experimental conditions to develop an understanding of structure-function relationships that dictate the physicochemical properties of vanadium oxide assemblies. Complex selection was dictated by two criteria – (1) nuclearity of the transition metal complexes (2) distribution of electron density in the native electronic configuration. Our analyses establish that electronic communication between metal centers significantly impacts charge transfer kinetics of these vanadium-based compounds.

Introduction

A synthetic chemist's ability to design molecules with unique structural, magnetic, and electronic properties opens pathways to tailor systems for optimal performance in desired applications. For many chemical processes, identifying strategies that leverage unique reactivities to compensate for intrinsic energetic deficiencies by either lowering the barrier to electron transfer or modifying reaction pathways can bolster their efficiency. Towards this end, utilizing redox active compounds that can effectively mediate chemical transformations by lowering the overpotential required for a given set of reactions is a powerful approach. Redox mediators are ions, molecules, or compounds that can undergo reversible oxidation and/or reduction reactions during an electrochemical reaction. These species often exhibit tunable (multi)redox properties, excellent stability, and fast electron transfer kinetics. For example, organic aminoxyls can be used as mediators for alcohol oxidation reactions under electrochemical conditions.[1] Semmelhack and coworkers have demonstrated the utility of TEMPO (2,2,6,6-tetramethylpiperidine N-oxyl) in undergoing facile electron transfer kinetics to yield successful oxidation of primary alcohols under mildly basic conditions.[2] Moreover, redox mediators can move the chemical reactions away from the electrode surface. This, in turn, prevents corrosion at the electrode surface thereby increasing the robustness of the system.

The design of efficient redox mediators is a murky territory as their practical applications are primarily identified through a "guess-and-check" approach. Often, only the (electro)chemical potential of the redox shuttle is considered, overlooking the plausible role of structural modifications in altering the kinetics of the electrochemical process. Thus, identifying redox mediators with modular structure-function properties that result in accelerated rates of electron transfer by overcoming high energetic demands is imperative for the success of many chemical and biological processes. Some key characteristics that are desirable in effective redox mediators include (1) stability and solubility across different oxidation states (2) reversible electrochemistry (3) high diffusivity (4) fast electron transfer kinetics (**Figure 1**).

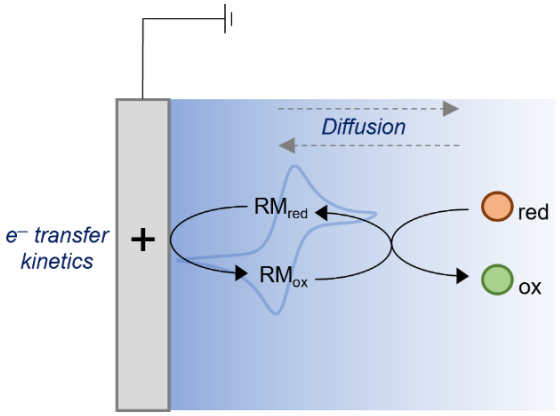

Figure 1. Design criteria for effective redox mediators (RMs) for chemical transformations – reversible electrochemistry, high diffusivity, facile electron transfer kinetics.

One class of compounds that serve as efficient redox mediators are organometallic complexes that exhibit delocalization of charge density. For example, Spokoyny and coworkers have demonstrated that multicenter bonding and electron delocalization in dodecaborane clusters can be utilized to achieve spatial separation of conjugated polymer polarons and

This article is protected by copyright. All rights reserved

15213765, 2024, 32, Downloaded from https://chemistry-europe.onlinelibrary.wiley.com/doi/10.1002/chem.202400764 by Office Of Scientific And Technical Information, Wiley Online Library on [20/08/2025]. See the Terms and Conditions (https://onlinelibrary.wiley.com/terms-and-conditions) on Wiley Online Library for rules of use; OA articles are governed by the applicable Creative Commons License

Author Manuscript

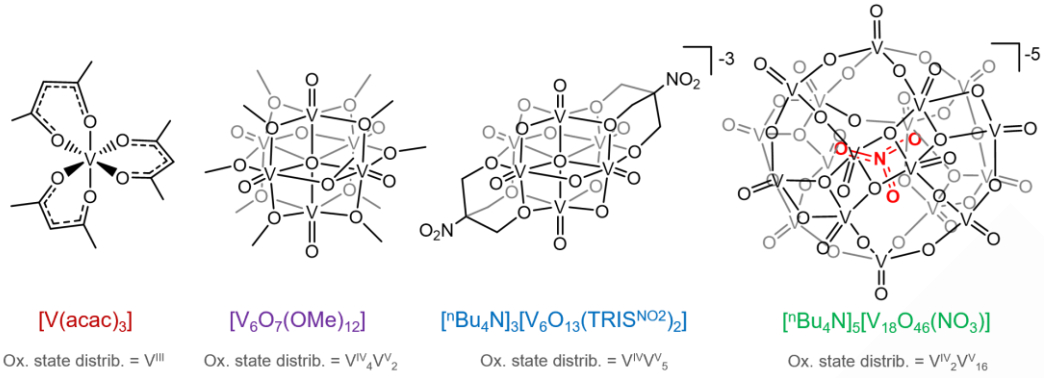

Figure 2. Vanadium complexes used in the present study for evaluating the dynamics of electron transfer across different metal oxide cores.

counterions, leading to highly delocalized and mobile charge carriers even in poorly crystalline polymer materials.[3] In another study, Tyson et al. have described that charge delocalization in p-toluidine allows it to serve as a redox mediator that can catalyze otherwise inefficient photooxidation of thiols to key thiyl radical intermediate.[4]

Polyoxometalates (POMs) can also function as good redox mediators owing to their multiple, reversible redox couples. Indeed, the electrochemical profiles of some POMs encompass wide potential ranges that provide opportunities to exploit reactivities with low overpotential.[5] Moreover, reduced POMs often exhibit delocalized electron structures that increase the overlap between electronic states, thus leading to facile charge transfer.[6] With this unique attribute in mind, our group[7] and others[8] have investigated the application of these multimetallic systems as redox mediators, leveraging electron transfer processes that result in (de)population of delocalized molecular orbitals via electronic communication between the metal centers. We have demonstrated that polyoxovanadate-alkoxide (POV-alkoxide) clusters exhibit electron transfer rate constants that are at least an order of magnitude faster than that of mononuclear transition metal complexes reported for nonaqueous flow-battery applications.[7a] The bridging alkoxide ligands allow for the negotiation of electron transfer events for the assembly at mild redox potentials, while increasing the solubility of the cluster in organic solvent across all charge states. While we have provided extensive evidence that POV-alkoxides exhibit excellent electrokinetic properties in non-aqueous media that are at par with the most promising charge carriers reported in literature,[9] the impetus of these fast electron transfer rate constants has not been explicitly investigated.

Herein, we report the effect of structural modifications on the heterogeneous electron transfer dynamics of molecular vanadium oxide architectures (**Figure 2**). We investigate the changes in reorganization energy of POV-alkoxide clusters to evaluate whether energetic costs are mitigated by electronic communication in multimetallic systems. We also assess the role of delocalized electron density in influencing the rates of charge transfer. Our results demonstrate that both nuclearity of the cluster assembly and delocalization of electron density contribute to the rapid electron transfer kinetics. Our findings highlight the critical role of electronic communication between metal centers in POV-alkoxides. We anticipate that these results will serve to inspire further studies in studying structure-function relationships to systematically design potent redox mediators for a diverse set of chemical transformations.

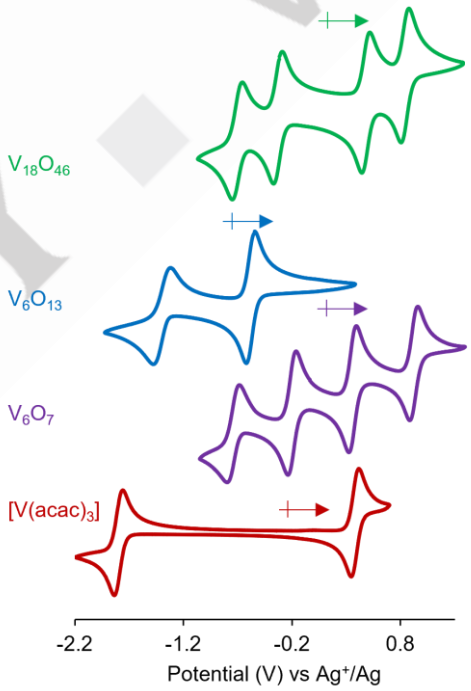

Figure 3. Cyclic voltammograms for the studied vanadium complexes. $[V(acac)_3]$ (red), $[V_6O_7(OCH_3)_{12}]$ (purple), $[V_6O_{13}(TRIS^{NO2})_2]^{3-}$ (blue), and $[V_{18}O_{46}(NO_3)]^{5-}$ (green) collected in acetonitrile with 0.1 M $[^nBu_4N][PF_6]$ as the supporting electrolyte (100 mV/s). The arrows indicate the corresponding open circuit potential (OCP) for each compound.

Results and Discussion

Diffusivity of Vanadium Complexes

An excellent redox mediator is completely soluble in the given solvent and exhibits good diffusion through solution (i.e. high diffusion coefficient). As such, it is pertinent to evaluate the diffusivity of the redox mediator in the prospective electrolyte system. While it is reasonable to hypothesize that increased size

This article is protected by copyright. All rights reserved

15213765, 2024, 32, Downloaded from https://chemistry-europe.onlinelibrary.wiley.com/doi/10.1002/chem.202400764 by Office Of Scientific And Technical Information, Wiley Online Library on [20/08/2025]. See the Terms and Conditions (https://onlinelibrary.wiley.com/terms-and-conditions) on Wiley Online Library for rules of use; OA articles are governed by the applicable Creative Commons License

Author Manuscript

and/or ligand density might inhibit mass transport for these systems, previous work from our lab has shown that diffusivity remains relatively unchanged for POV-alkoxide clusters with aliphatic ligand substitution of various carbon-chain lengths (e.g. $[V_6O_7(OCH_3)_{12}]$ vs. $[V_6O_7(OC_5H_{11})_{12}]$).[7a, 10] These findings suggested that the transport properties in redox mediators can often depend on more complex interactions between redox active species and solvent.

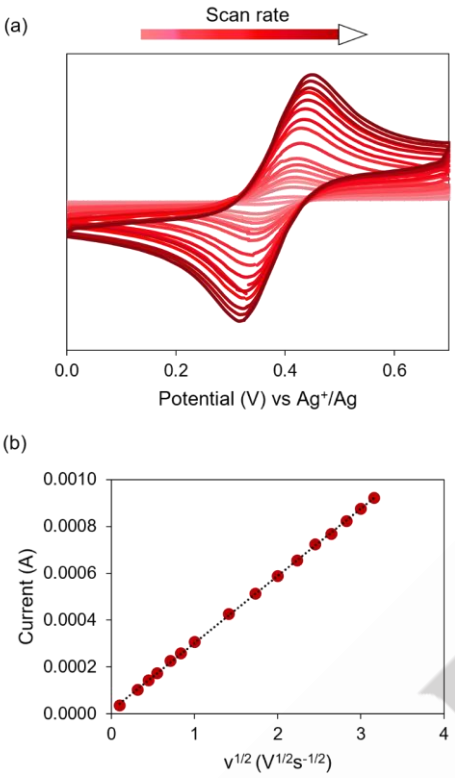

Figure 4. (a) Representative CV measurements of **O1** redox couple of 5 mM $[V(acac)_3]$ with 0.1 M $[^nBu_4N][PF_6]$ in MeCN at scan rates ranging from 10 – 10000 mV/s; (b) Randles-Sevcik analysis of the corresponding data.

$[V(acac)_3]$ has garnered widespread attention in the scientific community as an efficient redox mediator in Li-O_2 batteries due to its ability to mediate efficient oxidation of Li_2O_2 as well as accelerate O_2 reduction kinetics.[11] While several studies have reported the electrochemical behavior of $[V(acac)_3]$, we were interested in investigating the performance of this complex under identical experimental conditions to the multimetallic vanadium complexes reported here. $[V(acac)_3]$ was selected as the model monometallic complex due to its pseudo-octahedral coordination geometry, with a primary coordination sphere composed solely of oxygen atoms. The diffusion coefficient of $[V(acac)_3]$ was determined using the Randles-Sevcik method; the oxidation and reduction events were isolated (Scheme S1) and cyclic voltammograms were recorded at scan rates ranging from 10 – 10000 mV/s (**Figure 4**). The plot of the peak current (i_p) versus the square root of scan rate ($v^{1/2}$) exhibits a linear dependence, consistent with a diffusion-limited electrochemical process. The diffusion coefficients obtained for $[V(acac)_3]$ (D_0 for one electron oxidation, **O1** = 1.29 ± 0.37 × 10^{-5} cm^2 s^{-1}; and one electron reduction, **R1** = 1.36 ± 0.20 × 10^{-5} cm^2 s^{-1}) on glassy carbon surface are an order of magnitude faster than those previously reported (Figure S2 and S3).[12] We attribute this acceleration in mobility to a combined effect of the solvent and supporting electrolyte medium; $[^nBu_4N][PF_6]$ is used as the supporting electrolyte in MeCN instead of $[Et_4N][BF_4]$. The former salt yields smaller solvated species that decrease the solution resistance and results in faster diffusivity of the redox mediator.[13] Moreover, a key difference in our experimental work is that we employ scan rates up to 10000 mV/s, values that are much faster than the sweep rates previously used for electroanalytical measurements on $[V(acac)_3]$.[14] This, in turn, allows us to obtain a true estimate of the upper bound of diffusion coefficients of $[V(acac)_3]$, as well as other multimetallic vanadium oxide complexes studied in this work.

Next, we evaluated the diffusion behavior of the two hexavanadate clusters, and compared these values to the monometallic complex, $[V(acac)_3]$. Our investigations were governed by the hypothesis that although delocalization of electron density in clusters will accelerate the kinetics of charge transfer, the increased size of the assembly will result in decreased diffusivity. We selected the hexavanadium clusters, $[V_6O_7(OCH_3)_{12}]$ and $[^nBu_4N]_3[V_6O_{13}(TRIS^{NO2})_2]$ for investigation; while both clusters possess equal number of vanadium atoms, they differ in the identity and density of organic ligands bound to the cluster core (**Figure 2**). As depicted in **Figure 5** (Figures S4-S9), the observed diffusion coefficients for $[V_6O_7(OCH_3)_{12}]$ (**O1** = 7.82 ± 0.33 × 10^{-5} cm^2 s^{-1}, **R1** = 9.26 ± 0.12 × 10^{-6} cm^2 s^{-1}) are faster as compared to $[^nBu_4N]_3[V_6O_{13}(TRIS^{NO2})_2]$ (**O1** = 4.40 ± 0.22 × 10^{-6} cm^2 s^{-1}, **R1** = 2.65 ± 0.43 × 10^{-6} cm^2 s^{-1}). The diffusion coefficients of both hexavanadate assemblies are slower than $[V(acac)_3]$.

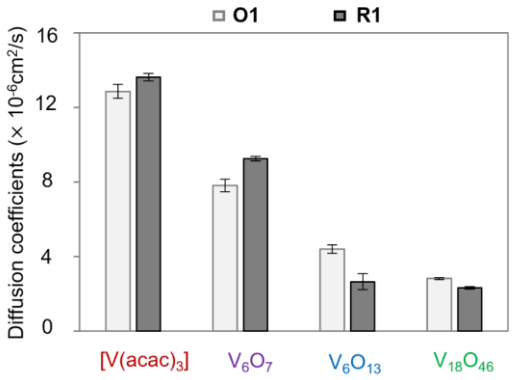

Figure 5. Diffusivity observed for the one electron oxidation (**O1)** and one electron reduction (**R1**) of the vanadium complexes on glassy carbon electrode surface. (V_6O_7 = $[V_6O_7(OCH_3)_{12}]$, V_6O_{13} = $[^nBu_4N]_3[V_6O_{13}(TRIS^{NO2})_2]$, $V_{18}O_{46}$ = $[^nBu_4N]_5[V_{18}O_{46}(NO_3)]$).

With interest in elucidating the consequences of surface ligation on the diffusivity of POV-alkoxides, we compared the D_0 values for the two hexavanadate clusters – $[V_6O_7(OCH_3)_{12}]$ and $[^nBu_4N]_3[V_6O_{13}(TRIS^{NO2})_2]$. The experimentally measured diffusion coefficients are slightly slower for $[^nBu_4N]_3[V_6O_{13}(TRIS^{NO2})_2]$. We attribute this behavior to the fact

This article is protected by copyright. All rights reserved

15213765, 2024, 32, Downloaded from https://chemistry-europe.onlinelibrary.wiley.com/doi/10.1002/chem.202400764 by Office Of Scientific And Technical Information, Wiley Online Library on [20/08/2025]. See the Terms and Conditions (https://onlinelibrary.wiley.com/terms-and-conditions) on Wiley Online Library for rules of use; OA articles are governed by the applicable Creative Commons License

Author Manuscript

that the latter assembly possess tridentate ligands with nitro substituents on opposite faces of the cluster that elongates the diameter of the cluster (10.075 Å) in comparison to $[V_6O_7(OCH_3)_{12}]$ (8.772 Å). Following the Stokes-Einstein relationship, the increased molecular radius slows the diffusion of the charged species to and from the electrode surface.

Finally, we looked at the octadecavanadate assembly, $[^nBu_4N]_5[V_{18}O_{46}(NO_3)]$, reported by Anjass and Streb.[15] In contrast to the other studied POV-alkoxide systems, this cluster exclusively possesses μ_2-O^{2-} ligands bridging vanadium centers. The result is a cage-like molecular structure where the metal oxide assembly hosts a nitrate ion. Our interest in this compound stemmed from its rich redox chemistry and large size. The cyclic voltammogram of the octadecavanadate cluster with 0.1 M $[^nBu_4N][PF_6]$ in MeCN possesses four quasi-reversible redox events ($E_{1/2}$ = −0.64, −0.30, +0.46, +0.80 V vs. Ag/$AgNO_3$). The open circuit voltage at −0.19 V (vs. Ag/$AgNO_3$) is positioned at the center of the redox processes observed in this window and describes a mixed-valent oxidation state distribution of vanadium ions ($V_2^V V_{16}^{IV}$). To be consistent with the evaluation of other multimetallic polyoxovanadates described in this work, we focused our attention on the one electron oxidation (**O1**; $E_{1/2}$ = +0.46 V) and reduction (**R1**; $E_{1/2}$ = − 0.30 V) processes of $[^nBu_4N]_5[V_{18}O_{46}(NO_3)]$. Measurement of the relevant redox processes of $[^nBu_4N]_5[V_{18}O_{46}(NO_3)]$ at variable scan rates (v = 10 – 10000 mV/s) reveals a linear correlation between i_p and $v^{1/2}$, similar to the other vanadium complexes studied in this work (Figure S10 – S12). The calculated D_0 values for **O1** and **R1** of $[^nBu_4N]_5[V_{18}O_{46}(NO_3)]$ are 2.82 ± 0.05 × 10^{-6} cm^2 s^{-1} and 2.33 ± 0.08 × 10^{-6} cm^2 s^{-1}, respectively. These values indicate that the diffusivity of the octadecavanadium compound is slowest amongst the series of complexes, consistent with its large size (diameter = 11.486 Å).

While the size of the cluster is identified as the predominant factor in governing the diffusivity of the vanadium complexes based on the Stokes-Einstein relationship, overall charge on the molecule can also affect the observed diffusion behavior. Indeed, electrophoretic effect can be operative in charged electrolyte solutions. As such, the movement of ions in solution can be correlated to charge on the complex. For instance, the observed diffusion coefficients for $[V_6O_{13}(TRIS^{NO2})_2]^{4-}$ (**R1** for $[^nBu_4N]_3[V_6O_{13}(TRIS^{NO2})_2]$) is similar to that observed for $[V_{18}O_{46}(NO_3)]^{4-}$ (**O1** for $[^nBu_4N]_5[V_{18}O_{46}(NO_3)]$). While both clusters differ in size, the charge on these assemblies is the same. Based on these observations, we infer that both size and charge have significant effect on the diffusion behavior of the studied vanadium complexes.

Heterogeneous Electron Transfer Rate Constants (k_0) of Vanadium Compounds

A defining characteristic of an effective redox mediator is its ability to efficiently shuttle electrons between the heterogeneous (electrode-mediator) and homogeneous (mediator-substrate) cascades. In this regard, rapid electron transfer rate constants are imperative. Redox mediators can significantly reduce kinetic constraints associated with sluggish charge transfer between different phases by lowering the required overpotential(s). This attenuation of kinetic energy is often achieved by two key attributes of redox mediators – (1) inter-atomic electron delocalization, and (2) number of sites available for delocalization. The extent of delocalization of electron density is an emergent design trait that aids in pivoting away from energetically demanding pathways. Thus, we became interested in mapping structure-function relationships of the vanadium complexes studied to understand the impact of nuclearity and electronic delocalization on the rate constants of electron transfer.

We began our investigations by comparing the heterogeneous rates of electron transfer between $[V(acac)_3]$ and $[V_6O_7(OMe)_{12}]$. Our motivation behind this comparison stems from our hypothesis that delocalization of electron density in multinuclear species will accelerate the kinetics of charge transfer. It should be noted that the oxidation states of vanadium involved in the redox chemistry of $[V(acac)_3]$ (**O1** = V^{III}/V^{IV}, **R1** = V^{III}/V^{II}) and $[V_6O_7(OMe)_{12}]$ (**O1** = V^{IV}/V^{V}, **R1** = V^{V}/V^{IV}) are different. We point this out, as the discrepancy in oxidation states of vanadium accessed in the redox couples may have an impact on the observed kinetic behavior. Our decision to study this monometallic complex was rooted in its pseudo-octahedral coordination geometry at vanadium, which is analogous to that observed for each of the vanadium centers contained within the hexavanadate assembly. In the context of this work, we are only probing the one electron oxidation/reduction processes (inner redox events) for $[V_6O_7(OMe)_{12}]$ (**Scheme 2**), as opposed to outermost redox events displayed in **Figure 3**, to avoid complications pertaining to stepwise vs. concerted multi-electron transfer pathways or cluster decomposition. Using the Nicholson method, we determined the rate constants for both species. As depicted in **Figure 6** (Figure S13 – S16), the oxidation and reduction kinetics of $[V_6O_7(OMe)_{12}]$ (**O1** = 8.48 ± 1.90 × 10^{-2} cm s^{-1}, **R1** = 5.31 ± 0.46 × 10^{-2} cm s^{-1}) are faster than those of $[V(acac)_3]$ (**O1** = 4.52 ± 0.53 × 10^{-2} cm s^{-1}, **R1** = 2.57 ± 0.32 × 10^{-2} cm s^{-1}).

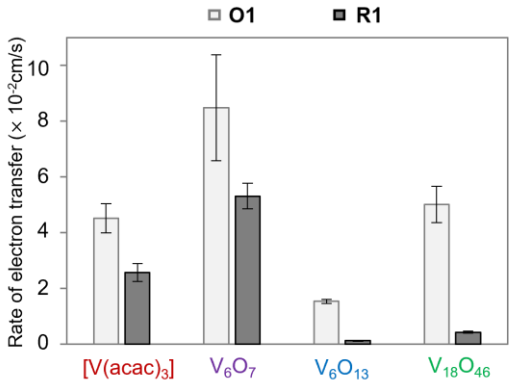

Figure 6. Heterogeneous electron transfer rate constants for one-electron oxidation (**1^+/0**) and reduction (**0/1^-**) of the vanadium complexes on glassy carbon electrode surface. (V_6O_7 = $[V_6O_7(OCH_3)_{12}]$, V_6O_{13} = $[^nBu_4N]_3[V_6O_{13}(TRIS^{NO2})_2]$, $V_{18}O_{46}$ = $[^nBu_4N]_5[V_{18}O_{46}(NO_3)]$).

To better understand the discrepancy of electron transfer rate constants in these systems, we evaluated the changes in the bond metrics of $[V(acac)_3]$ and $[V_6O_7(OMe)_{12}]$. The motivation behind this analysis is our expectation that structural changes

This article is protected by copyright. All rights reserved

15213765, 2024, 32, Downloaded from https://chemistry-europe.onlinelibrary.wiley.com/doi/10.1002/chem.202400764 by Office Of Scientific And Technical Information, Wiley Online Library on [20/08/2025]. See the Terms and Conditions (https://onlinelibrary.wiley.com/terms-and-conditions) on Wiley Online Library for rules of use; OA articles are governed by the applicable Creative Commons License

Author Manuscript

during oxidation/reduction will be reflected in the reorganization energies required for the electron transfer event. Hence, quantifying the changes in bond lengths and angles of these molecules during the redox processes will help develop an estimation of the reorganization energy in each system. It is important to note that this form of analysis probes pertinent bond metrics in the solid-state, which may not be wholly representative of the changes observed in solution (phase relevant to the electrochemical phenomenon interrogated in this work). Nonetheless, we present this information as a qualitative model for changes in V-O bond distances and O-V-O bond angles that may contribute to activation barriers that impede electron transfer at the electrode surface. We also note that we are only discussing changes in bond distances and angles between the neutral and cationic species (relevant structures for **O1**), as there is no crystal structure reported for $[V(acac)_3]^-$.

The crystal structure of $[V(acac)_3]$ has been previously reported by Montgomery and coworkers, whereas Hambley et al. have established that of $[V(acac)_3]^+$.[16] **Table 1** summarizes the bond metrics obtained for the neutral and cationic charge states of the compound. The average $V-O$ bond length in neutral $[V(acac)_3]$ is 1.979(8) Å, whereas upon oxidation to $[V(acac)_3]^+$ it reduces to 1.907(2) Å. Thus, V−O bond distances are shortened by ~4% upon oxidation. Furthermore, while the cis O−V−O bond angles only varies by 0.1º ± 0.06º, the trans O−V−O bond angles differ by 3º ± 0.10º (1.7%). Collectively, these changes in bond distances and angles represent significant structural perturbations that are observed upon oxidation of $[V(acac)_3]$.

Table 1. Select average bond distances and angles of $[V(acac)_3]$, $[V(acac)_3]SbCl_6$, $[V_6O_7(OMe)_{12}]$, $[V_6O_7(OMe)_{12}]SbCl_6$. (O_b = O atom of bridging alkoxide ligands, O_t = terminal oxo ligand of vanadyl moieties, O_c = O atom positioned at the center of the cluster)

Bond parameter	$[V(acac)_3]$	$[V(acac)_3]$ $SbCl_6$	$[V_6O_7(OMe)_{12}]$	$[V_6O_7(OMe)_{12}]$ $SbCl_6$
V−O	1.979(8) Å	1.907(2) Å	–	–
$V-O_c$	–	–	2.291(2) Å	2.277 Å
$V-O_b$	–	–	1.973(2) Å	1.958(3) Å
$V=O_t$	–	–	1.592(2) Å	1.577(2) Å
O–V–O (cis)	90.1(6)º	90.2(1)º	–	–
O−V−O (trans)	176.1º	173.4(1)º	–	–
$V-O_b-V$	–	–	110.3(8)º	110.6(9)º

In contrast, comparison of bond distances and angles at the vanadium centers of $[V_6O_7(OMe)_{12}]$ in its neutral and oxidized forms reveal almost no variation. For analysis, we used the crystal structure information files reported by Hartl and coworkers for complexes $[V_6O_7(OMe)_{12}]$ and $[V_6O_7(OMe)_{12}]^+$.[17] The average bond lengths of the vanadium atoms to the central μ^6-oxo ligand ($V-O_c$) is 2.291(2) Å in the neutral cluster whereas 2.277 Å (no error has been reported for this bond length in the crystal structure) in the positively charged state. Thus, $V-O_c$ bond distances in $[V_6O_7(OMe)_{12}]$ are shortened by only ~0.6% upon oxidation. Similarly, the average bond distance of vanadium centers to the bridging oxide ligands ($V-O_b$) varies by only 0.016(4) Å (0.7 %). The average bond length of the vanadium atoms to the terminal oxo ligand ($V=O_t$) is 1.592(2) Å for the neutral assembly whereas 1.577(2) Å for the one electron oxidized species (0.9 %). Lastly, changes in the $V-O_b-V$ angles are negligible (~0.35(9)º, 0.3%).

The bond metric analysis performed above confirms that the changes in bond distances and angles in the POV-alkoxide are significantly less than those observed upon of $[V(acac)_3]$. These observations suggest that the change in reorganization energies at individual vanadium centers during the oxidation of the hexavanadate cluster are less than those experienced by the single vanadium center in the monometallic species. Reorganization energies contribute to the total activation barrier for a redox reaction. This barrier determines the rate at which the reaction proceeds ─ lower reorganization energy leads to a lower activation barrier and consequently, a faster reaction. The increased nuclearity of the cluster can possibly explain the enhanced kinetic behavior of oxidation of $[V_6O_7(OMe)_{12}]$ in comparison to $[V(acac)_3]$.

Another plausible reason for the accelerated electrokinetics is charge delocalization amongst multiple vanadium centers in the POV-alkoxide cluster. To this end, bond valence sum (BVS) calculations were performed to assess the extent of delocalization in such assemblies. In mixed valent compounds, BVS calculations are a preferred method to determine the oxidation state of a given element. Deviations from whole number valences are attributed to delocalization of unpaired electrons to an extent that corresponds to the degree of the observed discrepancy. Indeed, BVS calculations illustrate that each vanadium center in $[V_6O_7(OMe)_{12}]$ is only partially oxidized (ΔBVS = +0.17) upon formation of $[V_6O_7(OMe)_{12}]^+$ (Table S1). These observations are in correspondence to the characteristic behavior of Robin and Day class II delocalized electronic structure of homometallic POV-alkoxide clusters where the cooperative electronic interaction between the vanadium ions facilitates electron transfer in and out of the system, with no significant changes to the molecular structure of the cluster core.[18] Thus, the minimal change in the geometry of the POV-alkoxide coupled with electronic communication between the V centers leads to lower energetic penalties in reorganization and ultimately improves the heterogeneous rates of electron transfer. In comparison, BVS calculations for the vanadium centers in $[V(acac)_3]$ and $[V(acac)_3]^+$ show localized valences of V^{III} and V^{IV}, respectively (Table S2).

Finally, we probed changes in kinetics as a function of electrode material; these experiments are critical for establishing inner vs. outer sphere mechanisms that are important because of thermodynamic reasons. Establishing the differences between these electron transfer mechanisms enable to choose the most

This article is protected by copyright. All rights reserved

15213765, 2024, 32, Downloaded from https://chemistry-europe.onlinelibrary.wiley.com/doi/10.1002/chem.202400764 by Office Of Scientific And Technical Information, Wiley Online Library on [20/08/2025]. See the Terms and Conditions (https://onlinelibrary.wiley.com/terms-and-conditions) on Wiley Online Library for rules of use; OA articles are governed by the applicable Creative Commons License

Author Manuscript

suitable approach to achieve optimal performance, efficiency, and control within the reaction system. Inner-sphere electron transfer processes are expected to be faster than most processes following an outer sphere electron transfer mechanism. These reactions are highly sensitive to the electrode material and the kinetics of electron transfer can vary significantly depending on the surface composition of the working electrode.[19] As such, we measured the rate constants of charge transfer on gold electrodes for $[V(acac)_3]$ and $[V_6O_7(OMe)_{12}]$ to determine the mechanism of charge transfer (Table S3, Figure S17 – S24). Our results indicate that the rate constants for $[V(acac)_3]$ change significantly as a function of electrode material, confirming that electron transfer between the electrode and $[V(acac)_3]$ redox mediator proceeds via an inner sphere electron transfer pathway. In contrast, no significant changes were observed in the electrokinetics of $[V_6O_7(OMe)_{12}]$ upon altering the electrode surface to gold; this observation is consistent with electron transfer proceeding through an outer-sphere mechanism. It is remarkable that the electron transfer kinetics are faster for the homoleptic hexavanadate despite following an outer sphere mechanism. We attribute this fact to the long-range electronic communication as well as the presence of bridging alkoxide ligands that can facilitate charge transfer. Overall, understanding the distinct mechanisms of electron transfer in redox mediated processes is vital for making informed choices about using them for suitable applications. However, in cases of chemical transformations where inner sphere electron transfer is not desirable (such as solvent sensitive reactions) but fast charge transfer is a pre-requisite, $[V_6O_7(OMe)_{12}]$ presents as an excellent redox mediator.

To probe the impact of delocalization in more depth, we compared two POV-alkoxide clusters – $[V_6O_7(OMe)_{12}]$ and $[^nBu_4N]_3[V_6O_{13}(TRIS^{NO2})_2]$. Both clusters have six vanadium atoms in the core. The ground state electronic configuration of $[^nBu_4N]_3[V_6O_{13}(TRIS^{NO2})_2]$ is $V^{IV}V_5^V$. The cyclic voltammogram of the cluster (**Figure 3**) exhibits two reversible redox waves corresponding to one electron oxidation (V_6^V) and the reduction event results from the injection of an additional electron into the hexavanadate core ($V_2^{IV}V_6^V$). In contrast, the homoleptic cluster $[V_6O_7(OMe)_{12}]$ is mixed valent in both its oxidized ($V_3^{IV}V_3^V$) and reduced forms ($V_5^{IV}V^V$). Both clusters have delocalized electronic structures, confirmed by the presence of intervalence charge transfer (IVCT) in the electronic absorption spectra of these clusters.[20] The major difference between the hexavanadate assemblies is the nature of the bridging ligands. $[^nBu_4N]_3[V_6O_{13}(TRIS^{NO2})_2]$ possess μ_2-O^{2-} bridging ligands as opposed to μ_2-CH_3O^- ligands in $[V_6O_7(OMe)_{12}]$ (**Figure 2**). Due to higher electronegativity of oxide ligands, they tend to pull electron density away from the vanadium center, reducing its ability to interact with other vanadium atoms in the polyoxovanadate. As depicted in **Figure 6** (Figure S25 – S26), the oxidation kinetics of $[^nBu_4N]_3[V_6O_{13}(TRIS^{NO2})_2]$ (k_0 = 1.53 ± 0.08 × 10^{-2} cm/s) is inhibited as compared to $[V_6O_7(OMe)_{12}]$ (k_0 = 8.48 ± 1.90 × 10^{-2} cm/s), despite the fact that the cluster possesses the same number of vanadium atoms. The heterogeneous rate constants of electron transfer are also smaller for **R1**. We ascribe this behavior to reductive instability of the reduced form of the POV-alkoxide cluster, $[^nBu_4N]_4[V_6O_{13}(TRIS^{NO2})_2]$, that might contribute to complex degradation and sluggish electron transfer kinetics.

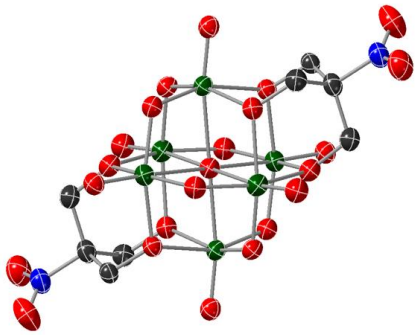

Figure 7. Molecular structure of $[CoCp^*_2][^nBu_4N]_2[V_6O_{13}(TRIS^{NO2})_2]$ shown with 50% probability ellipsoids. Counter cations (e.g. $[CoCp^*_2]^+$, $[^nBu_4N]^+$), solvent molecules, and hydrogen atoms have been removed for clarity. Key: dark green ellipsoids: V; red ellipsoids: O; blue ellipsoids: N; dark grey ellipsoids: C.

To account for the effect of structural perturbations on the electrokinetic behavior, we compared the bond distances and angles at the vanadium centers of V_6O_{13} in its 2- and 3- charged states. For analysis, we used the crystal structure information file reported by Zubieta and coworkers for complex $[V_6O_{13}(TRIS^{NO2})_2]^{2-}$.[20b] The crystal structure of $[V_6O_{13}(TRIS^{NO2})_2]^{3-}$ was obtained by our laboratory, and is included in **Figure 7** (Table S4). It should be noted that Zubieta and coworkers have generated this cluster electrochemically to perform EPR studies; however, no crystal structure has been reported yet. The average bond lengths of the vanadium atoms to the central μ^6-oxo ligand ($V-O_c$) is 2.244 Å (no error has been reported for this bond length in the crystal structure) in the 2- charged state whereas 2.252 Å (no error has been reported for this bond length in the crystal structure) in the 3- oxidation state. Thus, $V-O_c$ bond distances in V_6O_{13} are truncated by ~0.4% upon reduction. Similarly, the average bond distance of vanadium centers to the bridging oxide ligands ($V-O_b$) varies by only 0.006(3) Å (0.3 %, **Table 2**). The average bond length of the vanadium atoms to the terminal oxo ligand ($V=O_t$) is 1.602(2) Å for the 2- charged state whereas 1.613(4) Å for the reduced species (0.6 %). Lastly, changes in the $V-O_b-V$ angles are almost negligible (0.7(2)º, 0.6%). These structural perturbations are analogous to the $[V_6O_7(OMe)_{12}]$ (*vide supra*). These results indicate that the heterogeneous rate constants of electron transfer are not a reflection of the changes in geometry of the cluster core and highlight the importance of bridging alkoxides in facilitating charge transfer reactions.

While the inductive effect of the bridging ligands (μ_2-O^{2-} versus μ_2-CH_3O^-) can impact the kinetic behavior of the hexavanadate assemblies, it solely cannot induce such remarkable differences in the rate constants. Thus, we further probed the mechanism of electron transfer by employing Au surface as the working electrode and measured the kinetics of $[^nBu_4N]_3[V_6O_{13}(TRIS^{NO2})_2]$ (Figure S27 – S30). Our results indicate that there is a ten-fold decrease in the rate constants, confirming that $[^nBu_4N]_3[V_6O_{13}(TRIS^{NO2})_2]$ follows an inner sphere charge transfer pathway (Table S5). Thus, $[V_6O_7(OMe)_{12}]$ and

This article is protected by copyright. All rights reserved

15213765, 2024, 32, Downloaded from https://chemistry-europe.onlinelibrary.wiley.com/doi/10.1002/chem.202400764 by Office Of Scientific And Technical Information, Wiley Online Library on [20/08/2025]. See the Terms and Conditions (https://onlinelibrary.wiley.com/terms-and-conditions) on Wiley Online Library for rules of use; OA articles are governed by the applicable Creative Commons License

Author Manuscript

$[^nBu_4N]_3[V_6O_{13}(TRIS^{NO2})_2]$ follow different mechanistic charge transfer pathways. These results, in conjunction with those observed for $[V(acac)_3]$, indicate that the kinetics of $[V_6O_7(OMe)_{12}]$ trumps that of $[^nBu_4N]_3[V_6O_{13}(TRIS^{NO2})_2]$ and $[V(acac)_3]$ despite following an outer-sphere mechanism. We attribute this behavior to the contribution of bridging alkoxide ligands in facilitating charge transfer reactions. Furthermore, it is plausible that the presence of bulky ligands (acetylacetonate and tris(hydroxymethyl)methane) render the vanadium sites inaccessible for simple outer sphere reactions to and from the electrode surface.

Table 2. Select average bond distances and angles of $[V_6O_{13}(TRIS^{NO2})_2]^{2-}$, $[V_6O_{13}(TRIS^{NO2})_2]^{3-}$. ($O_b$ = O atom of bridging alkoxide ligands, O_t = terminal oxo ligand of vanadyl moieties, O_c = O atom positioned at the center of the cluster)

Bond parameter	$[V_6O_{13}]^{2-}$	$[V_6O_{13}]^{3-}$
$V-O_c$	2.244 Å	2.252 Å
$V-O_b$	1.932(3) Å	1.938(3) Å
$V=O_t$	1.602(2) Å	1.613(4) Å
$V-O_b-V$	110.9(1)º	110.2(2)º

Based on our observations on the electrokinetic properties of clusters exhibiting differing mechanisms, we became interested to investigate whether the poor rates of electron transfer in such systems can be mitigated by the enhanced nucleation of the cluster core. To evaluate this hypothesis, we selected the mixed-valent, high-nuclearity POV, $[^nBu_4N]_5[V_{18}O_{46}(NO_3)]$. As first reported by Hiyashi and coworkers, this self-assembled, all inorganic cluster exhibits the electronic distribution as $V_2^{IV}V_{16}^{V}$ of the vanadium centers (Scheme S4).[21] The cluster exhibits a double helical V_8 ribbon between two square pyramidal $V^{IV}O_5$ units. The crystal structure shows that the two reduced V^{IV} sites are localized where the vanadium atoms have square pyramidal coordination environment. The lack of electronic delocalization in the cluster core renders this cluster as a suitable candidate to compare to the hexavanadate species, $[^nBu_4N]_3[V_6O_{13}(TRIS^{NO2})_2]$, which exhibits sluggish electron transfer kinetics. As demonstrated in **Figure 6** (Figure S31 – S32), we observe that there is approximately a 3-fold enhancement in the heterogeneous rates of electron transfer for $[^nBu_4N]_5[V_{18}O_{46}(NO_3)]$ (**O1** = $5.01 \pm 0.65 \times 10^{-2}$ cm/s, **R1** = $4.18 \pm 0.03 \times 10^{-3}$ cm/s) as compared to $[^nBu_4N]_3[V_6O_{13}(TRIS^{NO2})_2]$ (**O1** = $1.53 \pm 0.08 \times 10^{-2}$ cm/s, **R1** = $1.14 \pm 0.01 \times 10^{-3}$ cm/s). The enhanced rates are possibly due to the increased number of V sites in $[^nBu_4N]_3[V_6O_{13}(TRIS^{NO2})_2]$. Notably, the three-fold escalation in the kinetics of electron transfer corresponds to the three-fold increase in the number of vanadium sites. To further probe the mechanism of electron transfer, we performed kinetic analysis on Au surface (Figure S33 - S36). Our results indicate no significant change in the rate constants, confirming an outer sphere electron transfer reaction (Table S5). These results are in support of our previous observation that bulky ligands inhibit the outer-sphere pathway in these vanadium complexes (*vide supra*). As such, the octadecavanadate cluster with compact ligands follow outer sphere mechanism.

Contrastingly, the rate constants of electron transfer are still faster in $[V_6O_7(OMe)_{12}]$, a cluster that exhibits the highest degree of electronic communication. Bridging alkoxide ligands in the hexavanadate cluster not only facilitate charge transfer to and from the electrode surface, but also enable outer-sphere electron transfer pathways that are less susceptible to side reactions. These observations depict that while delocalization significantly aids in reducing the kinetic barriers to add or remove electrons from the cluster core, sluggish electron transfer kinetics in partially or fully localized systems can be improved by increasing the nuclearity of the cluster. This imposes a tradeoff between the desirable characteristics of a redox mediator – higher nuclearity results in decreased diffusivity of the redox mediator in solution, albeit accelerating the electrokinetics. As such, specific consideration must be given to each of these physicochemical properties to select the optimal mediator for desirable application(s).

Conclusion

The current strategies for energy conversion and storage often suffer from poor selectivity and efficiency due to stringent thermodynamic and kinetic requirements. Redox mediators, especially polynuclear assemblies, are attractive solutions to combat this problem due to their ability to act as freely diffusing electron shuttles with high reversibility and stability. The design of efficient redox mediators requires the optimization of several physicochemical properties in tandem. In this work, we discuss the role of nucleation, electronic communication, and ligand identity on the heterogeneous rates of electron transfer of V-based redox mediators. We demonstrate that the hexavanadate assembly, namely $[V_6O_7(OMe)_{12}]$, exhibits faster electron transfer kinetics than the monometallic complex, $[V(acac)_3]$. This result is surprising as the latter exhibits inner sphere electron transfer mechanism, which in theory should exhibit faster kinetics. We attribute this behavior to electronic communication between the vanadium sites of the polyoxovanadate, which boosts the electrokinetics by many folds. When the bridging alkoxide ligands in the hexavanadate cluster are substituted by bridging oxides and TRIS-pendant groups, the rates of charge transfer plummet significantly. This molecular modification can be systematically controlled, thus providing opportunities to define structure–activity relationships that govern POV's redox mediating ability. Furthermore, we assess the impact of extent of delocalization versus nucleation on the experimental rate constants. Our results highlight that in compounds that exhibit poor rates, increasing the number of metal centers can help in improving the charge transfer kinetics. Such scenarios present a quid pro quo relationship in the attainable traits of a given redox mediator – increased nuclearity results in lower diffusivity at the cost of faster kinetics. Overall, we anticipate that these results will motivate further efforts in elucidating design criteria that will serve to ultimately create robust, efficient, and targeted redox mediators for a diverse set of chemical transformations.

This article is protected by copyright. All rights reserved

15213765, 2024, 32, Downloaded from https://chemistry-europe.onlinelibrary.wiley.com/doi/10.1002/chem.202400764 by Office Of Scientific And Technical Information, Wiley Online Library on [20/08/2025]. See the Terms and Conditions (https://onlinelibrary.wiley.com/terms-and-conditions) on Wiley Online Library for rules of use; OA articles are governed by the applicable Creative Commons License

Author Manuscript

Experimental Section

General considerations. All manipulations were carried out in the absence of water and oxygen in a UniLab MBraun inert atmosphere glovebox under a dinitrogen atmosphere. Glassware was oven dried for a minimum of 4 hours and cooled in an evacuated antechamber prior to use in the glovebox. Acetonitrile (MeCN) was dried and deoxygenated on a Glass Contour System (Pure Process Technology, LLC) and stored over activated 3 Å molecular sieves purchased from Fisher Scientific. Subsequently, the water content in MeCN was measured using Karl-Fischer titration method and was found to be 11 ppm (averaged over three titrations). Tetrabutylammonium hexafluorophosphate ($[^nBu_4N][PF_6]$) was purchased from Sigma-Aldrich, recrystallized thrice using hot methanol, and stored under dynamic vacuum for a minimum of two days prior to use. $[V(acac)_3]$ was purchased from Sigma Aldrich and used as received. $[V_6O_7(OMe)_{12}]$, $[^nBu_4N]_2[V_6O_{13}(TRIS^{NO2})_2]$, and $[^nBu_4N]_5[V_{18}O_{46}(NO_3)]$ were synthesized according to literature precedent.[10] $[^nBu_4N]_3[V_6O_{13}(TRIS^{NO2})_2]$ was obtained via bulk reduction of $[^nBu_4N]_2[V_6O_{13}(TRIS^{NO2})_2]$ (Figure S1). All electrochemical experiments were conducted in the dry box using a Bio-Logic SP 150 potentiostat/galvanostat and the EC-Lab software suite.

Cyclic voltammetry. Cyclic voltammetry (CV) was performed using a three-electrode setup inside a nitrogen filled glove box (UniLab MBraun) using a Bio-Logic SP 150 potentiostat/galvanostat and the EC-Lab software suite. The concentration of each complex and $[^nBu_4N][PF_6]$ were kept at 5 mM and 100 mM, respectively, throughout all measurements. CVs were recorded using a 3 mm diameter glassy carbon or gold working electrode (CH Instruments, USA), a Pt wire auxiliary electrode (CH Instruments, USA), and a Ag/Ag^+ non-aqueous reference electrode with 0.01 M $AgNO_3$ in 0.1 M $[^nBu_4N][PF_6]$ in MeCN (BASi, USA). CVs were iR compensated at 95% with impedance taken at 100 kHz using the ZIR tool included within the EC-Lab software. The remaining 5% uncompensated resistance was accounted for by manual correction using the strategy described by Myland and Oldham.[11]

Determining D_0. The diffusion coefficient (D_0) associated with each redox couple was determined by using the slope of the peak current (i_p) versus the square root of scan rate $v^{1/2}$. The Randles – Sevcik equation was used to estimate the diffusion coefficients from CV data. For a reversible redox couple, the peak current is given by eqn (1):

$$i_p = 2.69 \times 10^5 \, n^{3/2} \, A \, c \, D_0^{1/2} \, v^{1/2} \qquad \text{Eqn (1)}$$

In eqn(1), n is the number of electrons transferred; A is the electrode area (0.0707 cm^2 for the glassy carbon working electrode); c is the bulk concentration of the active species; D_0 is the diffusion coefficient of the active species; v is the scan rate. For an irreversible redox couple, the peak current, is given by the eqn(2):

$$i_p = 2.99 \times 10^5 \, n^{3/2} \, \alpha^{1/2} A \, c \, D_0^{1/2} \, v^{1/2} \qquad \text{Eqn (2)}$$

where α is the charge transfer coefficient. For this study, α = 0.5.

For the redox couples that show quasi-reversible kinetics, relationships for both reversible and irreversible redox reaction are usually employed to determine the diffusion coefficients of such redox processes. Therefore, an average value of diffusion coefficient was approximated for a quasi-reversible redox couple using both equations 1 and 2.[7a, 12]

Calculation of k_0. The electron-transfer kinetics was estimated directly from CV measurements by using the Nicholson method.[13] The potential difference (ΔEp) of oxidation and reduction peaks were obtained at different scan rates. The transfer parameter, ψ, was extracted from the working curve constructed by Nicholson using ΔEp values. The standard heterogeneous charge-transfer rate constant, k_0, for a given electron transfer process was determined using eqn (3):

$$\Psi = v^{-1/2} k_0 \left({}^{\pi n F D_0}/_{RT} \right)^{-1/2} \qquad \text{Eqn (3)}$$

where n is the number of electrons transferred, F is the Faraday constant, D is the diffusion coefficient, v is the scan rate, R is the ideal gas constant and T is the temperature.

Supporting Information

The authors have cited additional references within the Supporting Information.[23, 25]

Acknowledgements

The authors would like to thank Dr. Montaha H. Anjass (Department of Chemistry, University of Sharjah) for providing $[^nBu_4N]_5[V_{18}O_{46}(NO_3)]$ cluster used in this study and Dr. Alex A. Fertig for crystallizing $[V_6O_{13}(TRIS^{NO2})_2]^{3-}$. This research was funded by the Chemical Sciences, Geosciences and Biosciences Division, Office of Basic Energy Sciences, Office of Science, U.S. Department of Energy, via Grant DE-SC0002106.

Keywords: Redox mediator • Polyoxovanadates • Kinetics • Mechanism • Electronic communication

This article is protected by copyright. All rights reserved

15213765, 2024, 32, Downloaded from https://chemistry-europe.onlinelibrary.wiley.com/doi/10.1002/chem.202400764 by Office Of Scientific And Technical Information, Wiley Online Library on [20/08/2025]. See the Terms and Conditions (https://onlinelibrary.wiley.com/terms-and-conditions) on Wiley Online Library for rules of use; OA articles are governed by the applicable Creative Commons License

Author Manuscript

[1] a) J. E. Nutting, M. Rafiee, S. S. Stahl, *Chemical Reviews* **2018**, *118*, 4834-4885; b) C. W. Anson, S. S. Stahl, *Chemical Reviews* **2020**, *120*, 3749-3786.

[2] a) M. F. Semmelhack, C. S. Chou, D. A. Cortes, *Journal of the American Chemical Society* **1983**, *105*, 4492-4494; b) M. F. Semmelhack, C. R. Schmid, D. A. Cortes, *Tetrahedron Letters* **1986**, *27*, 1119-1122.

[3] a) T. J. Aubry, J. C. Axtell, V. M. Basile, K. J. Winchell, J. R. Lindemuth, T. M. Porter, J. Y. Liu, A. N. Alexandrova, C. P. Kubiak, S. H. Tolbert, A. M. Spokoyny, B. J. Schwartz, *Advanced Materials* **2019**, *31*; b) T. J. Aubry, K. J. Winchell, C. Z. Salamat, V. M. Basile, J. R. Lindemuth, J. M. Stauber, J. C. Axtell, R. M. Kubena, M. D. Phan, M. J. Bird, A. M. Spokoyny, S. H. Tolbert, B. J. Schwartz, *Advanced Functional Materials* **2020**, *30*.

[4] E. L. Tyson, Z. L. Niemeyer, T. P. Yoon, *Journal of Organic Chemistry* **2014**, *79*, 1427-1436.

[5] a) T. Homewood, J. T. Frith, J. P. Vivek, N. Casañ-Pastor, D. Tonti, J. R. Owen, N. Garcia-Araez, *Chemical Communications* **2018**, *54*, 9599-9602; b) R. J. Liu, K. C. Cao, A. H. Clark, P. L. Lu, M. Anjass, J. Biskupek, U. Kaiser, G. J. Zhang, C. Streb, *Chemical Science* **2020**, *11*, 1043-1051; c) Z. Q. Li, L. W. Liu, C. H. Mao, C. K. Zhou, M. Q. Xia, Z. Shen, Y. Guo, Q. Wu, X. Z. Wang, L. J. Yang, Z. Hu, *Acta Chimica Sinica* **2023**, *81*, 620-626; d) Y. Zheng, X. X. Xu, *Acs Applied Materials & Interfaces* **2020**, *12*, 53739-53748.

[6] D. Balzer, I. Kassal, *Science Advances* **2022**, *8*.

[7] a) A. M. Kosswattaarachchi, L. E. VanGelder, O. Nachtigall, J. P. Hazelnis, W. W. Brennessel, E. M. Matson, T. R. Cook, *Journal of the Electrochemical Society* **2019**, *166*, A464-A472; b) L. E. Vangelder, M. Matson, Ellen, *Journal of Materials Chemistry A* **2018**, *6*, 13874-13882; c) L. E. VanGelder, B. E. Petel, O. Nachtigall, G. Martinez, W. W. Brennessel, E. M. Matson, *Chemsuschem* **2018**, *11*, 4139-4149; d) L. E. VanGelder, E. Schreiber, E. M. Matson, *Journal of Materials Chemistry A* **2019**, *7*, 4893-4902.

[8] a) J. J. J. Chen, M. A. Barteau, *Journal of Energy Storage* **2017**, *13*, 255-261; b) Y. Cao, J. J. J. Chen, M. A. Barteau, *Journal of Energy Chemistry* **2020**, *50*, 115-124; c) S. Amin, J. M. Cameron, J. A. Watts, D. A. Walsh, V. Sans, G. N. Newton, *Molecular Systems Design & Engineering* **2019**, *4*, 995-999.

[9] a) B. Liu, C. W. Tang, C. Zhang, G. C. Jia, T. S. Zhao, *Chemistry of Materials* **2021**, *33*, 978-986; b) K. Gong, Q. R. Fang, S. Gu, S. F. Y. Li, Y. S. Yan, *Energy & Environmental Science* **2015**, *8*, 3515-3530.

[10] B. E. Schurr, O. Nachtigall, L. E. VanGelder, J. Drappeau, W. W. Brennessel, E. M. Matson, *Journal of Coordination Chemistry* **2019**, *72*, 1267-1286.

[11] a) Q. Zhao, N. Katyal, I. D. Seymour, G. Henkelman, T. Y. Ma, *Angewandte Chemie-International Edition* **2019**, *58*, 12553-12557; b) Y. Y. Dou, Z. J. Xie, Y. J. Wei, Z. Q. Peng, Z. Zhou, *National Science Review* **2022**, *9*.

[12] a) Q. H. Liu, A. E. S. Sleightholme, A. A. Shinkle, Y. D. Li, L. T. Thompson, *Electrochemistry Communications* **2009**, *11*, 2312-2315; b) A. A. Shinkle, A. E. S. Sleightholme, L. T. Thompson, C. W. Monroe, *Journal of Applied Electrochemistry* **2011**, *41*, 1191-1199; c) T. Herr, P. Fischer, J. Tubke, K. Pinkwart, P. Elsner, *Journal of Power Sources* **2014**, *265*, 317-324.

[13] S. Ahmadpour, J. Tashkhourian, B. Hemmateenejad, *Journal of Electroanalytical Chemistry* **2020**, *871*.

[14] a) Y. C. Yan, R. Walser-Kuntz, M. S. Sanford, *Acs Materials Letters* **2022**, *4*, 733-739; b) Y. C. Yan, L. Y. Zhang, R. Walser-Kuntz, D. B. Vogt, M. S. Sigman, G. H. Yu, M. S. Sanford, *Chemistry of Materials* **2022**, *34*, 10594-10605.

[15] S. Greiner, J. Hettig, A. Laws, K. Baumgartner, J. Bustos, A. C. Poppler, A. H. Clark, M. Nyman, C. Streb, M. Anjass, *Angewandte Chemie-International Edition* **2022**, *61*.

[16] a) B. Morosin, H. Montgomery, *Acta Crystallographica Section B* **1969**, *25*, 1354-1359; b) T. W. Hambley, C. J. Hawkins, T. A. Kabanos, *Inorganic Chemistry* **1987**, *26*, 3740-3745.

[17] C. Daniel, H. Hartl, *Journal of the American Chemical Society* **2005**, *127*, 13978-13987.

[18] M. Parthey, M. Kaupp, *Chemical Society Reviews* **2014**, *43*, 5067-5088.

[19] A. J. Bard, *Journal of the American Chemical Society* **2010**, *132*, 7559-7567.

[20] a) A. A. Fertig, S. M. G. Rabbani, M. D. Koch, W. W. Brennessel, P. Miro, E. M. Matson, *Nanoscale* **2021**, *13*, 6162-6173; b) Q. Chen, D. P. Goshorn, C. P. Scholes, X. L. Tan, J. Zubieta, *Journal of the American Chemical Society* **1992**, *114*, 4667-4681.

[21] Y. Koyama, Y. Hayashi, K. Isobe, *Chemistry Letters* **2008**, *37*, 578-579.

[22] Deposition numbers 2333681 (for $[CoCp^*_2][^nBu_4N]_2[V_6O_{13}(TRIS^{NO2})_2]$), These data are provided free of charge by the joint Cambridge Crystallographic Data Centre and Fachinformationszentrum Karlsruhe Access Structures service.

[23] CrysAlisPro, version 171.40.71a; Rigaku Corporation: Oxford, UK, 2020.

[24] Sheldrick, G. M. SHELXT, version 2018/2; Acta. Crystallogr. 2015, A71, 3-8.

[25] Sheldrick, G. M. SHELXL, version 2018/3; Acta. Crystallogr. 2015, C71, 3-8.

This article is protected by copyright. All rights reserved

15213765, 2024, 32, Downloaded from https://chemistry-europe.onlinelibrary.wiley.com/doi/10.1002/chem.202400764 by Office Of Scientific And Technical Information, Wiley Online Library on [20/08/2025]. See the Terms and Conditions (https://onlinelibrary.wiley.com/terms-and-conditions) on Wiley Online Library for rules of use; OA articles are governed by the applicable Creative Commons License

Author Manuscript

Entry for the Table of Contents

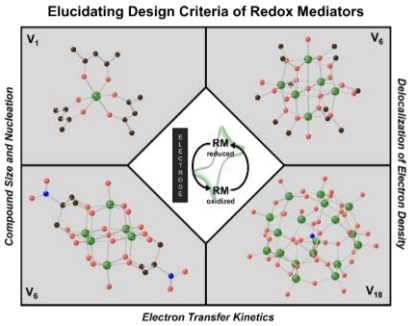

Insert text for Table of Contents here. Structure function relationships of vanadium oxide complexes (V_1 = $[V(acac)_3]$; V_6 = $[V_6O_7(OMe)_{12}]$ or $[V_6O_{13}(TRIS^{NO2})_2]^{-3}$; V_{18} = $V_{18}O_{46}(NO_3)]^{-5}$) in acetonitrile that dictate heterogeneous rate constants. Elucidation of design criteria for redox mediators.

Institute and/or researcher Twitter usernames: @MatsonLab

This article is protected by copyright. All rights reserved

15213765, 2024, 32, Downloaded from https://chemistry-europe.onlinelibrary.wiley.com/doi/10.1002/chem.202400764 by Office Of Scientific And Technical Information, Wiley Online Library on [20/08/2025]. See the Terms and Conditions (https://onlinelibrary.wiley.com/terms-and-conditions) on Wiley Online Library for rules of use; OA articles are governed by the applicable Creative Commons License

Author Manuscript